RSC Advances

ROYAL SOCIETY OF CHEMISTRY

www.rsc.org/advances

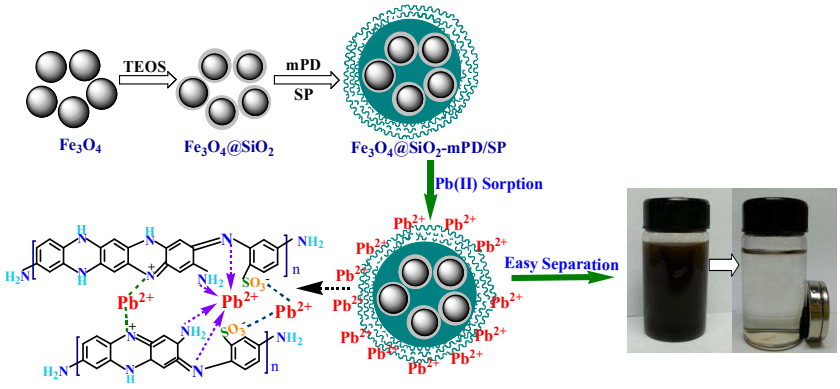

Multifunctional nanocomposites Fe_3O_4@SiO_2-mPD/SP for selective removal of Pb(II) and Cr(VI) from aqueous solutions

Lisha Tan, Jiang Xu, Xiaoqin Xue, Zhimo Lou, Jin Zhu, Shams Ali Baig, Xinhua Xu*

Department of Environmental Engineering, Zhejiang University, Hangzhou 310058, People's Republic of China

Abstract: Silica-coated magnetite (Fe_3O_4@SiO_2) nanoparticles functionalized with amino, imino and sulfonic groups (Fe_3O_4@SiO_2-mPD/SP) were successfully synthesized via a facile chemical oxidative polymerization of *m*-phenylenediamine (mPD) and *m*-sulfophenylenediamine-4-sulfonic acid (SP) monomers, and utilized for selective removal of Pb(II) and Cr(VI) from aqueous solutions. It was revealed by the characterizations that the polymers formed on Fe_3O_4@SiO_2 nanoparticles were the true copolymers with a mPD-SP unit, rather than a mixture of mPD and SP homopolymers. Fe_3O_4@SiO_2-mPD/SP nanocomposites could be easily separated from aqueous solutions within 30 s. The maximum adsorption capacity of Pb(II) (83.23 mg g^{-1}) and Cr(VI) (119.06 mg g^{-1}) on Fe_3O_4@SiO_2-mPD/SP nanocomposites were obtained at the mPD/SP molar ratio of 95:5 and 50:50, respectively. Moreover, satisfactory selective removal of Pb(II) and Cr(VI) from their mixtures with Cu(II) and Ni(II) ions were exhibited by the Fe_3O_4@SiO_2-mPD/SP(95:5) and Fe_3O_4@SiO_2-mPD/SP(50:50), respectively. The Pb(II) adsorption equilibrium was reached within 5 min by Fe_3O_4@SiO_2-mPD/SP(95:5). The adsorption data of Pb(II) and Cr(VI) were both fitted well to the Freundlich isotherm and followed the pseudo-second-order kinetic model. The adsorption mechanism of Pb(II) and Cr(VI)

on Fe_3O_4@SiO_2-mPD/SP nanocomposites included five processes, namely: ion-exchange, complexation adsorption, reduction reaction, electrostatic attraction and physical adsorption. The enhanced adsorption performance of nanoparticle-based magnetic adsorbents for selective removal of heavy metal ions can be achieved with such a copolymerization strategy.

Keywords: Fe_3O_4@SiO_2; Functionalization; Magnetic; Heavy metals; Adsorption

* Corresponding author. E-mail: xuxinhua@zju.edu.cn

1. Introduction

A variety of adsorption techniques have been extensively used to remove heavy metals from water, due to the advantages of high efficiency, low cost, and ease of operation. Various adsorbents have been developed for the removal of heavy metals from different water environments, including activated carbon, biosorbent materials, industrial waste, mineral adsorbents and nanofibers etc.[1-7]. However, some shortages have limited their practical applications in wastewater treatment, such as poor selectivity and regeneration potential, a strong tendency to produce secondary pollution, and difficult to achieved fast and efficient separation from aqueous solutions after adsorption.

Recently, magnetic nanoparticles such as Fe_3O_4 and γ-Fe_2O_3 have been investigated to remove heavy metals from contaminated aqueous environments[8-10]. These magnetic nanoparticles not only possess good performance which could be ascribed to the high surface area and optimal magnetic properties, but also can be rapidly recollected via external magnetic field and used repeatedly with low loss[11,12.] To improve the adsorption performance of Fe_3O_4 magnetic nanoparticles (Fe_3O_4 MNPs) toward heavy metals, an increasing number of investigations have been concentrating on the modification of Fe_3O_4 MNPs with different functional groups in recent years. For instance, the amino-functionalized Fe_3O_4 MNPs modified with (3-amine propyl) triethoxysilane[13,14], 1,6-hexadiamine[15], diethylenetriamine[16], 1,2-diaminobenzene[17] and ethylenediamine[18] showed excellent adsorption performance toward Pb(II), Cr(VI), Cu(II), Cd(II), As(III) and Cr(III). Thiol-functionalized Fe_3O_4 MNPs prepared using (3-mercaptopropyl) triethoxysilane[19] and dimercaptosuccinic acid[20] can effectively remove Hg(II) and Pb(II) ions. Carboxy-terminated Fe_3O_4[21], multi-functionalized Fe_3O_4 MNPs coated by

organic molecules such as humic acid[22], cetyltrimethylammonium bromide[23] and rhodamine hydrazide[24] were used as highly effective magnetic adsorbents for the removal of metal ions. The good performance of these magnetic adsorbents indicated that the large number of active sorption sites is vital and necessary for the efficient adsorption of heavy metal ions from aqueous solutions, which are provided by the free functional groups grafted on the Fe_3O_4 MNPs.

Polymer sorbents with functional groups have attracted more attention as new efficient sorbents of the metal ions, due to their excellent adsorbability and good selectivity toward the heavy metal ions[25-27]. In particular, copolymer sorbents of m-phenylenediamine/its sulfonate (mPD/SPD) and aniline/sulfoanisidine (AN/SA) both exhibit good thermal stability, remarkable chemical resistance, and excellent adsorbability for Pb(II), Hg(II) and Cr(VI) ions. This is mainly attributed to the introduction of sulfonic groups and the optimal combination of free amino, imino and sulfonic groups with different amounts. Moreover, the adsorbents can also be easily regenerated and reused through desorption[28, 29]. Polymer encapsulation provides the surface functionalization and protects the Fe_3O_4 MNPs from environmental disturbances. However, no studies using copolymer to modify Fe_3O_4@SiO_2 nanoparticles with amino/imino/sulfonic groups for selective removal of heavy metals have been reported so far. To the best of our knowledge, this is the first study of its kind to explore the effect of monomer ratio on the removal performance and discuss the adsorption mechanisms.

In this study, Fe_3O_4@SiO_2-mPD/SP magnetic nanocomposites were synthesized via chemical oxidative polymerization of *m*-phenylenediamine (mPD) and *m*-sulfophenylenediamine-4-sulfonicacid (SP). The effects of monomer ratio on the selective removal of Pb(II) and Cr(VI) ions from aqueous solutions were discussed.

Different characterization techniques were employed to investigate physico-chemical properties of Fe_3O_4@SiO_2-mPD/SP nanocomposites. The applicability of Fe_3O_4@SiO_2-mPD/SP in Pb(II) and Cr(VI) ions adsorption was evaluated with respect to its adsorption kinetics and isotherm. Additionally, the possible adsorption mechanisms of Pb(II) ions on Fe_3O_4@SiO_2-mPD/SP(95:5) and Cr(VI) ions on Fe_3O_4@SiO_2-mPD/SP(50:50) were also analyzed.

2. Materials and methods

2.1 Materials

$FeCl_3 \cdot 6H_2O$, $FeSO_4 \cdot 7H_2O$, $NH_3 \cdot H_2O$, polyethylene glycol 4000 (PEG4000), tetraethoxysilane (TEOS) and $(NH_4)_2S_2O_8$ were obtained from the Sinopharm Group Chemical Reagent Co., Ltd., China. mPD, $Pb(NO_3)_2$, and $K_2Cr_2O_7$ were purchased from Aladdin Reagent Co., Ltd., China. SP was purchased from Maya Chemical Reagent Co., Ltd., China. All chemicals were of analytical grade and used as received.

2.2 Preparation of Fe_3O_4@SiO_2-mPD/SP

Fe_3O_4 MNPs were firstly prepared by the co-precipitation method as reported previously[30] with a slight modification. Briefly, 4.7067 g $FeCl_3 \cdot 6H_2O$ and 3.025 g $FeSO_4 \cdot 7H_2O$ were dissolved in 50 mL PEG4000 solution (0.2 g mL^{-1}), then 10 mL $NH_3 \cdot H_2O$ mixed with 25 mL PEG4000 solution was added dropwise into the reaction mixture under nitrogen atmosphere with vigorous mechanical stirring for 2 h (60 ^oC). Afterward, the black precipitates were collected using a magnet and washed to neutral with deionized water.

Fe_3O_4@SiO_2 nanoparticles were synthesized via a sol-gel approach[31]. Typically,

the as-prepared Fe_3O_4 MNPs (~2 g) were homogeneously dispersed in a mixture of methyl alcohol (100 mL), deionized water (50 mL) and TEOS (1.76 mL) by sonicating for 30 min, followed by the addition of $NH_3 \cdot H_2O$ (4 mL). After 4 h continuous mechanical stirring at room temperature, Fe_3O_4@SiO_2 nanoparticles were magnetically separated, washed to neutral, and then dried in a vacuum oven at 60 ℃ for 12 h.

Fe_3O_4@SiO_2-mPD/SP nanocomposites were synthesized by chemical oxidative polymerization of mPD and SP in distilled water, using $(NH_4)_2S_2O_8$ as the oxidant. A typical procedure was as follows: Firstly, 0.5 g Fe_3O_4@SiO_2, 1 mmol mPD and 1 mmol SP were dispersed into 100 mL distilled water to form Solution 1. Secondly, Solution 2 was obtained by dissolving 2 mmol $(NH_4)_2S_2O_8$ into 10 mol distilled water. Both of the solutions were put into a water bath at 30 °C for 30 min. Thirdly, Solution 2 was added to the Solution 1 at a rate of one drop every 3 seconds with constant stirring at 30 ℃ for 24 h. The obtained black precipitates were magnetically separated, and washed repeatedly with distilled water. Lastly, the final products (Fe_3O_4@SiO_2-mPD/SP) were dried in a vacuum oven at 60 ℃ for 12 h.

2.3 Characterization

The morphology of the Fe_3O_4@SiO_2-mPD/SP nanocomposites was observed using transmission electron microscopy (TEM, JEM-1230, JEOL, Japan). Fourier transformed infrared spectra were recorded on an IR spectrophotometer (FTIR, IRaffinity-1, SHIMADZU, Japan) with KBr pellets at room temperature. The crystal structure of the particles was identified by X-ray diffraction (XRD, X'pert PRO,

155 analytical B.V., Netherlands). The binding energies were measured by X-ray
156 photoelectron spectroscopy (XPS, Kratos Axis Ultra DLD, SHIMADZU, Japan). The
157 thermal stability of the Fe_3O_4@SiO_2-mPD/SP was investigated via
158 thermo-gravimetric analysis (TGA, TGA/SDTA851, SWRTZER LAND, USA) at a
159 heating rate of 10 °C/min under N_2 flow. Magnetic measurements were obtained using
160 a multifunctional physical property measurement system (PPMS-9, QUANTUM
161 DESIGN, USA) under a magnetic field up to 20 kOe at 298 K.

162 **2.4 Adsorption experiments**

163 Adsorption of Pb(II) and Cr(VI) ions from aqueous solution was performed
164 through batch experiments. We set out to find out the optimum mPD/SP ratios for
165 Fe_3O_4@SiO_2-mPD/SP nanocomposites to remove Pb(II) and Cr(VI). The adsorption
166 kinetics and isotherms of Pb(II) adsorption using Fe_3O_4@SiO_2-mPD/SP(95:5) and
167 Cr(VI) adsorption by Fe_3O_4@SiO_2-mPD/SP(50:50) were also studied. Unless
168 otherwise noted, all the experiments were performed in duplicate in Erlenmeyer flasks,
169 which were placed in the water bath oscillators at 180 rpm for 24 h at 30 °C. After
170 magnetic separation, the final concentration of Pb(II) was determined by an atomic
171 absorption spectrophotometer (AAS, AA-6300, SHIMADZU, Japan), and the
172 remaining concentration of Cr(VI) was analyzed via an ultraviolet-visible
173 spectrophotometer (UV-vis, UV1800, Puxi, China).

174 **3. Results and discussion**

175 **3.1 Characterization of Fe_3O_4@SiO_2-mPD/SP**

Fig. 1 shows the XRD patterns of Fe_3O_4, Fe_3O_4@SiO_2, and Fe_3O_4@SiO_2-mPD/SP nanoparticles. Six diffraction peaks (220, 311, 400, 442, 511, and 440) were observed, indicating the presence of cubic spinel structure of pure magnetite[32]. The same characteristic peaks were observed for Fe_3O_4@SiO_2 and Fe_3O_4@SiO_2-mPD/SP nanoparticles, indicating that the crystalline structure of Fe_3O_4 was stable during silica coating and subsequent surface modification. Fig. 2 presents TEM images of the four nanoparticles. Fig. 2a shows that the Fe_3O_4 MNPs obtained by a modified co-precipitation method were composed of spherical and uniform particles with an average size of 20-30 nm. The dispersibility of Fe_3O_4@SiO_2 nanoparticles was improved after coating with a SiO_2 layer (Fig. 2b). However, it was difficult to observe the SiO_2 layer coated on Fe_3O_4, which could be the result of small amount of TEOS added into the reaction solution. As shown in Figs. 2c and 2d, it could be clearly observed that the mPD/SP copolymers with a thickness of ca. 8 nm were uniformly coated on Fe_3O_4@SiO_2 surface.

<Fig 1 about here>

<Fig 2 about here>

To identify the presence of silica and mPD/SP copolymers on Fe_3O_4 surface, the FTIR spectra of Fe_3O_4, Fe_3O_4@SiO_2, Fe_3O_4@SiO_2-mPD/SP(95:5), and Fe_3O_4@SiO_2-mPD/SP(50:50) were recorded (Fig. 3). The peaks at 592 and 1631 cm^{-1} were attributed to the Fe-O vibration from Fe_3O_4[33]. The characteristic peaks at 1083 and 802 cm^{-1} could be attributed to the asymmetric and symmetric stretching vibration of SiO_2, respectively. The vibration of SiO_2 as well as the weak bending vibration of Si-OH band at 964 cm^{-1} indicated the successful coating of silica shells on the surface of Fe_3O_4. A broad and strong peak centered at 3372 cm^{-1} was attributed to the characteristic N-H stretching vibration[27,34], which suggested the presence of a large

amount of amino and imino groups in the polymer-coating on Fe_3O_4 MNPs. The absorption peaks at 1622 and 1514 cm^{-1} were associated with the stretching of quinoid and benzenoid rings, respectively. The absorption peak at 1220 cm^{-1} was assigned to C-N vibration in mPD units in mPD/SP copolymers[29]. A peak at 1124 cm^{-1} could be attributed to the C-N stretching on the SP units, because the relative band intensity increases as the SP content rises from 5 to 50 mol%. The two absorptions at 1049 and 1020 cm^{-1} were associated with the S=O asymmetric and symmetric stretching vibration of the $-SO_3^-$ group on the SP units, respectively[25, 35, 36]. The peaks at 706 and 625 cm^{-1} correspond to the stretching vibration of C-S and S-O bonds on the SP units, respectively. The intensity of bands at 1124, 1049, 1020, and 706 cm^{-1} significantly rose with increasing SP unit content from 5% to 50%, which indicated the copolymers on the $Fe_3O_4@SiO_2$ were the true copolymers with a mPD-SP unit, rather than a mixture of mPD and SP homopolymers.

<Fig 3 about here>

TGA analyses were used to determine the content of organic functional copolymers coated on Fe_3O_4 MNPs. As shown in Fig. 4, weight loss at temperatures below 200 °C was assigned to the water desorption from the surface of $Fe_3O_4@SiO_2$-mPD/SP, while weight loss above 600 °C was caused by the loss of the structural water. The weight loss from 200 to 680 °C was associated with the decomposition of mPD/SP copolymers and silica layer grafted onto the Fe_3O_4, as well as two water loss. It suggested that the content of mPD/SP copolymers in the $Fe_3O_4@SiO_2$-mPD/SP(95:5) and $Fe_3O_4@SiO_2$-mPD/SP(50:50) were found to be about 31.05 and 32.82 wt.%, respectively. The saturation magnetization curves of Fe_3O_4, $Fe_3O_4@SiO_2$, $Fe_3O_4@SiO_2$-mPD/SP(95:5), and $Fe_3O_4@SiO_2$-mPD/SP(50:50) were shown in Fig. 5. The saturation magnetization value was 75.00 emu g^{-1}, 62.47

emu g^{-1}, 43.92 emu g^{-1}, and 41.33 emu g^{-1} for bare Fe_3O_4, Fe_3O_4@SiO_2, Fe_3O_4@SiO_2-mPD/SP(95:5), and Fe_3O_4@SiO_2-mPD/SP(50:50), respectively. Although the saturation magnetization decreased after surface modification, the adsorbents could still be easily separated from aqueous solution within 30 s. The content of mPD/SP copolymers coated on the Fe_3O_4@SiO_2 was found to be 29.69 wt.% for Fe_3O_4@SiO_2-mPD/SP(95:5) and 33.84 wt.% for Fe_3O_4@SiO_2-mPD/SP(50:50), which were consistent with those from TGA data.

<Fig 4 about here>

<Fig 5 about here>

3.2 Optimization of the mPD/SP ratio for the Fe_3O_4@SiO_2-mPD/SP as Pb(II) and Cr(VI) sorbents

Fig. 6a shows the adsorption capacity of Pb(II) on Fe_3O_4@SiO_2-mPD/SP nanocomposites modified with different mPD/SP feed ratios. The adsorption capacity was observed to strongly depend on the mPD/SP feed ratio. The Fe_3O_4@SiO_2-mPD/SP nanocomposites with SP content of 5 mol% (Fe_3O_4@SiO_2-mPD/SP(95:5)) demonstrated the maximum adsorption capacity of 82.95 mg g^{-1}, which was 16.78% higher than those of nanocomposites modified with pure mPD polymer. This might be attributed to the introduction of an optimal amount of active sulfonic groups on the copolymer chains coated on the Fe_3O_4@SiO_2 nanoparticles, which also led to loose conglomeration. However, the adsorption capacity was observed to decrease with the increasing SP content from 5 to 100 mol%, owing to a declined ion complexation. That is to say, the number of amino and imino groups per mass copolymer would decrease as the SP content increased, hence

reducing the probability of complexation between the copolymer chains and Pb(II)[29]. Additionally, the increased solubility of the copolymer due to the hydrophilicity of the sulfonic group could be another reason why the Pb(II) adsorbability declined with increasing SP content[37].

<Fig 6 about here>

As shown in Fig. 6b, the Cr(VI) adsorption capacity onto the Fe_3O_4@SiO_2-mPD/SP nanocomposites rose first and then decreased with the increasing SP content. Particularly, the Fe_3O_4@SiO_2-mPD/SP(50:50) nanocomposites were observed to possess the maximum adsorption capacity up to 118.53 mg g^{-1}, showing an enhancement of 59.46% and 67.08% as compared to pure mPD and SP, respectively. The enhancement of adsorbability might be attributed to the optimal combination of free amino, imino, and sulfonic groups on the copolymer chains at 50 mol% SP content, which was beneficial to the efficient interaction of Cr(VI) and the $=N-/=N^+H/-NH_2/-SO_3H$ groups[29]. Although the adsorption of Cr(VI) ions was similar to that of Pb(II), it should be noted that the Cr(VI) adsorbability decreased with increasing SP content from 50 to 100 mol%. This is because Cr(VI) exists as negatively charged $HCrO_4^-$ in aqueous solution, which would generate electrostatic repulsion force with $-SO_3^-$, leading to a decrease in adsorbability with an increasing SP content.

As shown in Fig. 6, the Pb(II) adsorption capacity onto the Fe_3O_4@SiO_2-mPD/SP(100:0) and Fe_3O_4@SiO_2-mPD/SP(0:100) were 71.03 and 52.64 mg g^{-1}, respectively. If the polymers coated on Fe_3O_4@SiO_2 were the mixture of

mPD homopolymers and SP homopolymers, the Pb(II) adsorption capacity onto Fe_3O_4@SiO_2-mPD/SP(95:5) should be about 70.11 mg g^{-1} (71.03×95%+52.64×5%= 70.11). Whereas, the actual Pb(II) adsorption capacity onto Fe_3O_4@SiO_2-mPD/SP (95:5) was 82.95 mg g^{-1}. And if the polymers were mixture, the Cr(VI) adsorption capacity onto Fe_3O_4@SiO_2-mPD/SP(50:50) should be about 72.64 mg g^{-1} (74.33×50%+70.95×50%=72.64). Whereas, the actual Cr(VI) adsorption capacity onto Fe_3O_4@SiO_2-mPD/SP(50:50) was 118.53 mg g^{-1}. It indicated that the polymers on the Fe_3O_4@SiO_2 were the true copolymers with a mPD-SP unit, rather than a simple mixture of mPD and SP homopolymers, which was consistent with the result of FTIR characterization.

3.3 Selective adsorption of metal ions

In order to investigate the selective adsorption of Fe_3O_4@SiO_2-mPD/SP nanocomposites, competitive adsorption of Pb(II), Cu(II) and Ni(II) on Fe_3O_4@SiO_2-mPD/SP(95:5) and Cr(VI), Cu(II) and Ni(II) on Fe_3O_4@SiO_2-mPD/SP(50:50) was performed, respectively. Since CrO_4^{2-} specie always existed in the Cr(VI) solution and would precipitate with Pb(II) to form $PbCrO_4$ due to the very small solubility product constant of $PbCrO_4$ ($K_{sp}=2.8\times10^{-13}$), the selective adsorption between Pb(II) and Cr(VI) was not performed. Fig. 7a shows the result of removal of Pb(II), Cu(II) and Ni(II) by Fe_3O_4@SiO_2-mPD/SP(95:5) with the same initial single ion concentration. The Pb(II) adsorption capacity onto the Fe_3O_4@SiO_2-mPD/SP(95:5) was 74.07 mg g^{-1}, while the adsorption capacity of Cu(II) and Ni(II) were only 7.44 and 4.18 mg g^{-1}, which was 9.96 times and 17.72 times

higher than the adsorption capacity of Cu(II) and Ni(II), respectively. It was revealed that the Fe_3O_4@SiO_2-mPD/SP(95:5) possessed excellent adsorbing selectivity towards Pb(II) in the presence of Cu(II) and Ni(II). The result of selective adsorption of Cr(VI) onto Fe_3O_4@SiO_2-mPD/SP(50:50) was presented in Fig. 7b. The Cr(VI) adsorption capacity onto the Fe_3O_4@SiO_2-mPD/SP(50:50) was 113.11 mg g^{-1}, while the adsorption capacity of Cu(II) and Ni(II) were only 13.60 and 8.56 mg g^{-1}, which was 8.32 times and 13.21 times higher than the adsorption capacity of Cu(II) and Ni(II), respectively. It was observed that the adsorption capacity of Fe_3O_4@SiO_2-mPD/SP(50:50) for Cr(VI) ions was much higher than that for Cu(II) and Ni(II) ions. In short, the Fe_3O_4@SiO_2-mPD/SP nanocomposites could be employed to efficiently and selectively remove hazardous Pb(II) and Cr(VI) ions from their mixtures with Cu(II) and Ni(II) ions.

<Fig 7 about here>

3.4 Adsorption kinetics

Fig. 8a presents the effect of contact time on Pb(II) uptake onto the Fe_3O_4@SiO_2-mPD/SP(95:5) nanocomposites. It was observed that adsorption rate was significantly high and rapidly reached an equilibrium after 5 min, which indicated that the Fe_3O_4@SiO_2-mPD/SP(95:5) exhibited faster Pb(II) adsorption than the other magnetic adsorbents[38-42]. The rapid adsorption could be attributed to the unique synergistic complexation between Pb(II) ions and amino/imino/sulfonic groups on the copolymers coated on Fe_3O_4@SiO_2[29]. In order to evaluate the mechanism of adsorption, pseudo-first-order and pseudo-second-order kinetics models[43,44] were used to describe the adsorption data. The pseudo-second-order kinetics equation of the

316 Pb(II) adsorption kinetics onto Fe_3O_4@SiO_2-mPD/SP(95:5) was presented in Fig. 8a
317 (inset) and Table 1, where q_e, and q_t were the adsorption capacities of Pb(II) ions
318 adsorbed (mg g^{-1}) at equilibrium and at time t (min), respectively; k_1 and k_2 were the
319 corresponding adsorption rate constants. On the basis of the high correlation
320 coefficient (R^2=1), the pseudo-second-order fitted perfectly with the experimental data,
321 suggesting that the rate-limiting step of adsorption was chemical adsorption between
322 sorbent and adsorbate without involvement of a mass transfer in solution[45,46]. The
323 experimental q_e value (83.23 mg g^{-1}) showed a good agreement with the calculated q_e
324 value (83.19 mg g^{-1}) derived from the pseudo-second-order kinetic.

325 *<Fig 8 about here>*

326 *<Table 1 about here>*

327 Fig. 8b presents the kinetics of Cr(VI) adsorption on the
328 Fe_3O_4@SiO_2-mPD/SP(50:50). The results illustrated that the Cr(VI) adsorption was
329 very fast during the initial 30 min and then gradually reached an equilibrium after 6 h.
330 The adsorption process consisted of two steps: the primary rapid step and the
331 secondary slow step. The primary rapid step of Cr(VI) sorption might be owing to the
332 reduction reaction and physical adsorption between Cr(VI) and functional groups.
333 While the secondary slow step might be controlled by the diffusion of the big $HCrO_4^-$
334 ions into inner functional groups within the copolymers as well as the electrostatic
335 repulsion between $HCrO_4^-$ and $-SO_3^-$. To investigate the adsorption process, the
336 pseudo-first-order and pseudo-second-order models were applied to the kinetics data.
337 As shown in Fig. 8b and Table 1, the adsorption kinetics was better described by the
338 pseudo-second-order model with a much higher correlation coefficient (R^2=0.9997).
339 Since the pseudo-second-order was based on the assumption that the chemical
340 adsorption between sorbent and adsorbate was the rate-controlling step[47], the Cr(VI)

adsorption mechanism on the Fe_3O_4@SiO_2-mPD/SP(50:50) was considered to mainly involve reduction reaction and subsequent complexation adsorption between Cr(III) and functional groups. The theoretical q_e value (119.76 mg g^{-1}) of pseudo second-order kinetics also agreed very well with the experimental q_e value (119.06 mg g^{-1}).

3.5 Adsorption isotherms

The adsorption isotherms of Pb(II) ions onto Fe_3O_4@SiO_2-mPD/SP(95:5) and Cr(VI) ions on Fe_3O_4@SiO_2-mPD/SP(50:50) were shown in Fig. 9a and 9b. The Langumir and Freundlich isotherm models were employed to describe the adsorption isotherms. The parameters of the isotherm models obtained from the corresponding fittings were listed in Table 2, where q_m represented the adsorption capacity, the Langmuir constant (k_L) represented the affinity between the adsorbent and adsorbate, the Freundlich constant (k_F) indicated the adsorption capacity, and n was the adsorption equilibrium constant related to adsorption intensity. Apparently, adsorption behaviors of Pb(II) ions by Fe_3O_4@SiO_2-mPD/SP(95:5) and Cr(VI) ions by Fe_3O_4@SiO_2-mPD/SP(50:50) were both better described by Freundlich model, which obtained a higher correlation coefficient than Langumir isotherms. The values of k_F (48.37, 59.56 $mg^{(1-1/n)}$ $L^{1/n}$ g^{-1}) and n (8.539, 5.968) indicated the easy separation of Pb(II) and Cr(VI) from liquid phase and favourable adsorption process ($1< n <10$)[48].

<Fig 9 about here>

<Table 2 about here>

3.6 Adsorption mechanism

The solution pH values were observed to drop from 4.35 to 4.13 after Pb(II) adsorption on Fe_3O_4@SiO_2-mPD/SP(95:5), which signified that the deprotonation

reaction happens on the amino/imino and sulfonic groups on the polymer chains, leading to the release of H^+ into the aqueous solution. That is to say, Pb(II) ions would be adsorbed by the protonated amino, imino, and sulfonic groups on Fe_3O_4@SiO_2 via ion-exchange, resulting in the release of H^+ into the aqueous solution. Although the solution pH values increased from 4.65 to 5.17 after Cr(VI) adsorption on Fe_3O_4@SiO_2-mPD/SP(50:50), the H^+ on protonated $-NH_2$, $-NH-$, and $-SO_3^-$ groups could also be exchanged with the Cr(III) cation ions produced by the redox reaction[29,49]. However, ion-exchange adsorption was not the main adsorption mechanism due to the limited amount of available H^+ on the copolymers.

The FTIR spectra of the Fe_3O_4@SiO_2-mPD/SP(95:5) and Fe_3O_4@SiO_2-mPD/SP(50:50) before (c, d) and after (e, f) adsorption of Pb(II) and Cr(VI) were presented in Fig. 3. The intensity of peaks at 1220 and 1124 cm^{-1} were observed to become weaker after the adsorption of Pb(II) and Cr(VI) ions, which were attributed to C-N stretching on the mPD and SP benzenoid rings, respectively. It indicated that the $-N=$,$-NH_2$ and $-NH-$ groups in the copolymers could chelate Pb(II) and Cr(III) ions to form stable chelating structures, where the Cr(III) was produced by the reduction reaction between the $-NH_2$/$-NH-$ groups and Cr(VI) ions. Noted that a strong new peak at 1383 cm^{-1} was observed in the FTIR spectrum of Fe_3O_4@SiO_2-mPD/SP(95:5) after Pb(II) adsorption (Fig. 3e), which was the characteristic peak for the stretching vibration of NO_2 in the NO_3^- ions[50,51]. Because NO_3^- ions was beneficial to balance the electrical charges of the adsorbed Pb(II) ions on the surface of Fe_3O_4@SiO_2-mPD/SP(95:5). Additionally, the introduced sulfonic groups in polymers could not only chelate heavy ions, but also form a ring with adjacent imino groups[28, 29]. Since the presence of stable chelating structures and a large amount of amino/imino/sulfonic groups in the copolymers, the complexation

adsorption was the main adsorption mechanism.

Fig. 10a shows the typical wide scan XPS spectra of Fe_3O_4@SiO_2-mPD/SP(50:50) before and after Cr(VI) adsorption. After Cr(VI) adsorption, new peaks around 580 eV emerged, which was designated to the photoelectron peaks of chromium, indicating the successful uptake of chromium on the Fe_3O_4@SiO_2-mPD/SP(50:50) surface[52]. Detailed XPS survey on the region of Cr2p was presented in Fig. 10b. Since the photoelectron peaks for Cr 2p 3/2 and 2p 1/2 centered at 577.1 and 586.8 eV, it was confirmed that Cr(III) ions was the predominant chromium species on the surface[53-55]. Because the amino and imino groups with strong reducibility could convert Cr(VI) into Cr(III) via a reduction reaction. Fig. 11a shows the variation of the total Cr and Cr(VI) residual concentration in the solutions with adsorption time. It can be observed that Cr(III) indeed formed upon adding the Fe_3O_4@SiO_2-mPD/SP(50:50) nanocomposites into the Cr(VI) solution, which indicated the occurrence of a redox reaction between the amino/imino groups as reductant and Cr(VI) ions as oxidant. That is to say, some of Cr(VI) were reduced to Cr(III) ions. FTIR spectra of Fe_3O_4@SiO_2-mPD/SP(50:50) before and after Cr(VI) adsorption are given in Fig. 3. After Cr(VI) adsorption, the intensity ratio of 1622 cm^{-1} over 1514 cm^{-1} became higher, which were associated with the stretching of quinoid and benzenoid rings, respectively. Thus, it indicated that a part conversion from benzenoid to quinoid structure because of a redox sorption of Cr(VI) on the nanoparticles. The variation of residual concentration of total Cr and Cr(VI) with adsorption time on Fe_3O_4 and Fe_3O_4@SiO_2 was also investigated. As shown in Fig. 11b, although the Cr(VI) could be reduced to Cr(III) by Fe(II), only a small amount of iron ions were leached out to the solution after Fe_3O_4 were coated with a SiO_2 layer and a polymer layer, which could be ignored.

<*Fig 10 about here*>

<*Fig 11 about here*>

At an initial solution of pH 4.65, the major Cr(VI) species ($HCrO_4^-$ and $Cr_2O_7^{2-}$ anions) could be adsorbed onto the copolymer through a strong electrostatic attraction between chromium anions and protonated amino/imino groups ($-NH_3^+-/-NH_2^+-$). After adsorption, sorbents were washed with deionized water and then separated by centrifugation for a few minutes. Consequently, the Pb(II) and Cr(VI) ions could be detected in the supernatants, which indicated that physical adsorption of Pb(II) and Cr(VI) on Fe_3O_4@SiO_2-mPD/SP existed but was not very prominent.

In summary, the probable adsorption mechanisms involved in this process included: ion-exchange, complexation adsorption, reduction reaction, electrostatic attraction and physical adsorption, as shown in Fig. 12.

<*Fig 12 about here*>

4. Conclusions

Novel Fe_3O_4@SiO_2-mPD/SP nanocomposites with high saturation magnetization and thermal stability were successfully synthesized and employed for the selective removal of Pb(II) and Cr(VI) ions from aqueous solutions. The adsorption of Pb(II) and Cr(VI) ions by Fe_3O_4@SiO_2-mPD/SP nanocomposites was found to be highly dependent on mPD/SP feed ratio. Fe_3O_4@SiO_2-mPD/SP(95:5) was the most efficient nanocomposites for Pb(II) adsorption with a fast adsorption equilibrium time (5 min), while Fe_3O_4@SiO_2-mPD/SP(50:50) showed the maximum adsorption capacity for Cr(VI) ions. The Fe_3O_4@SiO_2-mPD/SP(95:5) and Fe_3O_4@SiO_2-mPD/SP(50:50) nanocomposites could be employed to efficiently and selectively remove Pb(II) and

Cr(VI) from their mixtures with Cu(II) and Ni(II) ions, respectively. Both of the adsorption data fitted well to Freundlich isotherm model, and also agreed well with pseudo-second-order kinetics model. The maximum adsorption capacities of Pb(II) onto Fe_3O_4@SiO_2-mPD/SP(95:5) and Cr(VI) on Fe_3O_4@SiO_2-mPD/SP(50:50) were calculated to be 83.23 and 119.06 mg g^{-1}, respectively. The adsorption mechanism of Pb(II) and Cr(VI) on Fe_3O_4@SiO_2-mPD/SP nanocomposites included: complexation adsorption, reduction reaction, ion-exchange, electrostatic attraction and physical adsorption. The complexation adsorption was considered to be the primary adsorption mechanism for Pb(II) removal, while the complexation adsorption and reduction reaction were the main adsorption mechanisms for Cr(VI).

Acknowledgments

The authors acknowledge the financial support of the National Natural Science Foundation (No. 21477108, No. 21277119) and the Science and Technology Project of Zhejiang Province, China (No. 2012C23061).

References

1 F. Miyaji, S. Masuda, and Y. Suyama, *J. Ceram. Soc. Jpn.*, 2010, **118**, 1062-1066.

2 A. Demirbas, *J. Hazard. Mater.*, 2008, **157**, 220-229.

3 A. Chojnacki, K. Chojnacka, J. Hoffmann, and H. Gorecki, *Miner. Eng.*, 2004, **17**, 933-937.

4 S. Babel, and T. A. Kurniawan, *J. Hazard. Mater.*, 2003, **97**, 219-243.

458 5 P. A. Brown, S. A. Gill, and S. J. Allen, *Water Res.*, 2000, **34**, 3907-3916.

459 6 R. Wang, S. H. Guan, A. N. Sato, X. Wang, Z. Wang, R. Yang, B. S. Hsiao and B.
460 Chu, *J. Membrane Sci.*, 2013, **446**, 376-382.

461 7 R. Yang, K. B. Aubrecht, H. Y. Ma, R. Wang, R. B. Grubbs, B. S. Hsiao and B. Chu,
462 *Polymer*, 2014, **55,** 1167-1176.

463 8 P. Xu, G. M. Zeng, D. L. Huang, C. L. Feng, S. Hu, M. H. Zhao, C. Lai, Z. Wei, C.
464 Huang, G. X. Xie, and Z. F. Liu, *Sci. Total Environ.*, 2012, **424**, 1-10.

465 9 N. N. Nassar, *J. Hazard. Mater.*, 2010, **184**, 538-546.

466 10 J. Hu, G. H. Chen, and I. Lo, *Water Res.*, 2005, **39**, 4528-4536.

467 11 S. Tang, and I. Lo, *Water Res.*, 2013, **47**, 2613-2632.

468 12 Y. F. Shen, J. Tang, Z. H. Nie, Y. D. Wang, Y. Ren, and L. Zuo, *Bioresour. Technol.*,
469 2009, **100**, 4139-4146.

470 13 J. M. Zhang, S. R. Zhai, S. Li, Z. Y. Xiao, Y. Song, Q. D. An, and G. Tian, *Chem.*
471 *Eng. J.*, 2013, **215-216**, 461-471.

472 14 J. H. Wang, S. R. Zheng, Y. Shao, J. L. Liu, Z. Y. Xu, and D. Q. Zhu, *J. Colloid*
473 *Interface Sci.*, 2010, **349**, 293-299.

474 15 Y. Q. Tan, M. Chen, and Y. M. Hao, *Chem. Eng. J.*, 2012, **191**, 104-111.

475 16 S. H. Huang, and D. H. Chen, *J. Hazard. Mater.*, 2009, **163**, 174-179.

476 17 F. Zhang, J. Lan, Z. S. Zhao, Y. Yang, R. Q. Tan, and W. J. Song, *J. Colloid*
477 *Interface Sci.*, 2012, **387**, 205-212.

478 18 S. Singh, K. C. Barick, and D. Bahadur, *J. Hazard. Mater.*, 2011, **192**, 1539-1547.

479 19 O. Hakami, Y. Zhang, and C. J. Banks, *Water Res.*, 2012, **46**, 3913-3922.

20 W. Yantasee, C. L. Warner, T. Sangvanich, R. S. Addleman, T. G. Carter, R. J. Wiacek, G. E. Fryxell, C. Timchalk, and M. G. Warner, *Environ. Sci. Technol.*, 2007, **41**, 5114-5119.

21 Z. G. Feng, S. Zhu, D. de Godoi, A. Samia, and D. Scherson, *Anal. Chem.*, 2012, **84**, 3764-3770.

22 J. F. Liu, Z. S. Zhao, and G. B. Jiang, *Environ. Sci. Technol.*, 2008, **42**, 6949-6954.

23 Y. J. Jin, F. Liu, M. P. Tong, and Y. L. Hou, *J. Hazard. Mater.*, 2012, **227**, 461-468.

24 Z. Q. Wang, D. Y. Wu, G. H. Wu, N. N. Yang, and A. G. Wu, *J. Hazard. Mater.*, 2013, **244-245**, 621-627.

25 Q. F. Lu, M. R. Huang, and X. G. Li, *Chem. Eur. J.*, 2007, **13**, 6009-6018.

26 I. B. Kim, B. Erdogan, J. N. Wilson, and U. Bunz, *Chem. Eur. J.*, 2004, **10**, 6247-6254.

27 X. G. Li, M. R. Huang, W. Duan, and Y. L. Yang, *Chem. Rev.*, 2002, **102**, 2925-3030.

28 X. G. Li, H. Feng, and M. R. Huang, *Chem. Eur. J.*, 2009, **15**, 4573-4581.

29 M. R. Huang, H. J. Lu, and X. G. Li, *J. Mater. Chem.*, 2012, **22**, 17685-17699.

30 Y. S. Kang, S. Risbud, J. F. Rabolt, and P. Stroeve, *Chem. Mater.*, 1996, **8**, 2209.

31 Y. Cheng, R. Q. Tan, W. Y. Wang, Y. Q. Guo, P. Cui, and W. J. Song, *J. Mater. Sci.*, 2010, **45**, 5347-5352.

32 T. Z. Yang, C. M. Shen, Z. Li, H. R. Zhang, C. W. Xiao, S. T. Chen, Z. C. Xu, D. X. Shi, J. Q. Li, and H. J. Gao, *J. Phys. Chem. B*, 2005, **109**, 23233-23236.

33 R. Y. Hong, T. T. Pan, and H. Z. Li, *J. Magn. Mater.*, 2006 ,**303**, 60-68.

34 J. Yue, Z. H. Wang, K. R. Cromack, A. J. Epstein, and A. G. Macdiarmid, *J. Am. Chem. Soc.*, 1991, **113**, 2665-2671.

35 X. G. Li, R. Liu, and M. R. Huang, *Chem. Mater.*, 2005, **17**, 5411-5419.

36 M. T. Nguyen, P. Kasai, J. L. Miller, and A. F. Diaz, *Macromolecules*, 1994, **27**, 3625-3631.

37 Y. T. Xu, L. Z. Dai, J. F. Chen, J. Y. Gal, and H. H. Wu, *Eur. Polym. J.*, 2007, **43**, 2072-2079.

38 F. Ge, M. M. Li, H. Ye, and B. X. Zhao, *J Hazard. Mater.*, 2012, **211**, 366-372.

39 B. Guo, F. Deng, Y. Zhao, X. Luo, S. Luo, and C. Auc, *Appl. Surf. Sci.*, 2014, **292**, 438-446.

40 P. Xu, G. M. Zeng, D. L. Huang, C. Lai, M. H. Zhao, Z. Wei, N. J. Li, C. Huang, and G. X. Xie, *Chem. Eng. J.*, 2012, **203**, 423-431.

41 L. L. Fan, C. N. Luo, M. Sun, X. J. Li, and H. M. Qiu, *Colloid. Surface. B*, 2013, **103**, 523-529.

42 A. Idris, N. Ismail, N. Hassan, E. Misran, and A. F. Ngomsik, *J. Ind. Eng. Chem.*, 2012, **18**, 1582-1589.

43 Y. S. Ho, *J. Hazard. Mater.*, 2006, **136**, 681-689.

44 Y. S. Ho, and G. McKay, *Water Res.*, 1999, **33**, 578-584.

45 M. Yurdakoc, Y. Seki, S. Karahan, and K. Yurdakoc, *J. Colloid Interface Sci.*, 2005, **286**, 440-446.

46 F. C. Wu, R. L. Tseng, and R. S. Juang, *Water Res.*, 2001, **35**, 613-618.

47 Z. Aksu, *Sep. Purif. Technol.*, 2001, **21**, 285-294.

524 48 P. Figueira, C. B. Lopes, A. L. Daniel-da-Silva, E. Pereira, A. C. Duarte, and T.
525 Trindade, *Water Res.*, 2011, **45**, 5773-5784.
526 49 N. Akhtar, M. Iqbal, S. I. Zafar, and J. Iqbal, *J. environ. sci.-China*, 2008, **20**,
527 231-239.
528 50 M. Takafuji, S. Ide, H. Ihara, and Z. H. Xu, *Chem. Mater.*, 2004, **16**, 1977-1983.
529 51 C. K. Liu, R. B. Bai, and Q. S. Ly, *Water Res.*, 2008, **42**, 1511-1522.
530 52 A. R. Pratt, and N. S. McIntyre, *Surf. Interface Anal.*, 1996, **24**, 529-530.
531 53 N. Fiol, C. Escudero, and I. Villaescusa, *Bioresource Technol.*, 2008, **99**,
532 5030-5036.
533 54 X. Q. Li, J. S. Cao, and W. X. Zhang, *Ind. Eng. Chem. Res.*, 2008, **47**, 2131-2139.
534 55 Y. C. Li, Z. H. Jin, T. L. Li, and Z. M. Xiu, *Sci. Total Environ.*, 2012, **421**, 260-266.
535

Captions

Table 1 Kinetics model equations for Pb(II) and Cr(VI) adsorption on Fe_3O_4@SiO_2-mPD/SP(95:5) and Fe_3O_4@SiO_2-mPD/SP(50:50).

Table 2 Parameters of adsorption isotherms of Pb(II) and Cr(VI) adsorption on Fe_3O_4@SiO_2-mPD/SP(95:5) and Fe_3O_4@SiO_2-mPD/SP(50:50).

Fig. 1 XRD patterns of (a) Fe_3O_4, (b) Fe_3O_4@SiO_2, (c) Fe_3O_4@SiO_2-mPD/SP(95:5) and (d) Fe_3O_4@SiO_2-mPD/SP(50:50).

Fig. 2 TEM images of (a) Fe_3O_4, (b) Fe_3O_4@SiO_2, (c) Fe_3O_4@SiO_2-mPD/SP(95:5) and (d) Fe_3O_4@SiO_2-mPD/SP(50:50).

Fig. 3 FTIR spectra of (a) Fe_3O_4, (b) Fe_3O_4@SiO_2, (c) Fe_3O_4@SiO_2-mPD/SP(95:5), (d) Fe_3O_4@SiO_2-mPD/SP(50:50), (e) Fe_3O_4@SiO_2-mPD/SP(95:5) after adsorption of Pb(II), and (f) Fe_3O_4@SiO_2-mPD/SP(50:50) after adsorption of Cr(VI).

Fig. 4 TGA curves of Fe_3O_4@SiO_2-mPD/SP(95:5) and Fe_3O_4@SiO_2-mPD/SP(50:50).

Fig. 5 Magnetization curves of Fe_3O_4, Fe_3O_4@SiO_2, Fe_3O_4@SiO_2-mPD/SP(95:5) and Fe_3O_4@SiO_2-mPD/SP(50:50).

Fig. 6 (a) Pb(II) adsorptivity at an initial Pb(II) concentration of 100 mg L^{-1}, (b) Cr(VI) adsorptivity at an initial Cr(VI) concentration of 150 mg L^{-1} with the same 1 g L^{-1} Fe_3O_4@SiO_2-mPD/SP nanocomposites at 30°C for 24h.

Fig. 7 Selective adsorption of Pb(II) and Cr(VI) onto Fe_3O_4@SiO_2-mPD/SP nanocomposites: (a) adsorption of Cr(VI), Cu(II) and Ni(II) by Fe_3O_4@SiO_2-mPD/SP (50:50) at an initial single ion concentration of 100 mg L^{-1}, (b) adsorption of Cr(VI), Cu(II) and Ni(II) onto Fe_3O_4@SiO_2-mPD/SP (50:50) at an initial single ion concentration of 150 mg $L^{-1}$with the same 1 g L^{-1} Fe_3O_4@SiO_2-mPD/SP nanocomposites at 30°C.

561 **Fig. 8** Effect of contact time on Pb(II) adsorption onto Fe_3O_4@SiO_2-mPD/SP(95:5)
562 (a), and Cr(VI) adsorption on Fe_3O_4@SiO_2-mPD/SP(50:50) (b). Pb(II) initial
563 concentration = 100 mg L^{-1}, Cr(VI) initial concentration = 150 mg L^{-1},
564 Fe_3O_4@SiO_2-mPD/SP nanocomposites = 1 g L^{-1}, 30°C.
565 **Fig.9** Equilibrium isotherm for the Pb(II) adsorption onto Fe_3O_4@SiO_2-mPD/SP(95:5)
566 (a), and Cr(VI) adsorption on Fe_3O_4@SiO_2-mPD/SP(50:50) (b) with the same
567 1 g L^{-1} Fe_3O_4@SiO_2-mPD/SP nanocomposites at 30°C. The inset illustrates
568 the linear dependence of $\log q_e$ on $\log c_e$.
569 **Fig. 10** XPS wide survey for Fe_3O_4@SiO_2-mPD/SP(50:50) before and after Cr(VI)
570 adsorption (a). High-resolution XPS survey of Cr2p (b).
571 **Fig. 11** (a) The variation of residual concentration of total Cr and Cr(VI) with
572 adsorption time onto Fe_3O_4@SiO_2-mPD/SP(50:50). (b) The variation of
573 residual concentration of total Cr and Cr(VI) with adsorption time onto Fe_3O_4
574 and Fe_3O_4@SiO_2.
575 **Fig. 12** The possible Pb(II) and Cr(VI) adsorption mechanism on
576 Fe_3O_4@SiO_2-mPD/SP nanocomposites.
577

578 **Table 1** Kinetics model equations for Pb(II) and Cr(VI) adsorption on

579 Fe_3O_4@SiO_2-mPD/SP(95:5) and Fe_3O_4@SiO_2-mPD/SP(50:50).

Kinetics models	Equation	Correlation coefficient	Rate constant(k)	$q_{e,cal}$	$q_{e,exp}$
Pb(II) adsorption on Fe_3O_4@SiO_2-mPD/SP(95:5)					
Pseudo-2nd-order	$t/q_t = 0.01201t+2.32\times10^{-4}$	1	$k_2=0.6217$	83.26	83.23
Cr(VI) adsorption on Fe_3O_4@SiO_2-mPD/SP(50:50)					
Pseudo-1st-order	$\ln(q_e - q_t) = 3.81072 - 0.00115t$	0.8092	$k_1=1.15\times10^{-3}$	/	/
Pseudo-2nd-order	$t/q_t = 0.00835t+0.03945$	0.9997	$k_2=1.77\times10^{-3}$	119.76	119.06

[a] $q_{e,cal}$ = (mg g^{-1}), k_1= (min^{-1}), and k_2= (g mg^{-1} min^{-1}).

580

581

582 **Table 2** Parameters of adsorption isotherms of Pb(II) and Cr(VI) adsorption onto

583 Fe_3O_4@SiO_2-mPD/SP(95:5) and Fe_3O_4@SiO_2-mPD/SP(50:50).

Metal ions	Langmuir			Freundlich		
	K_L (L mg^{-1})	q_m (mg g^{-1})	R^2	K_F ($mg^{1-(1/n)}$ $L^{1/n}$ g^{-1})	n	R^2
Pb(II)	0.2418	86.43	0.8891	48.37	8.539	0.9980
Cr(VI)	0.04926	158.73	0.9504	59.56	5.968	0.9976

584

585

586

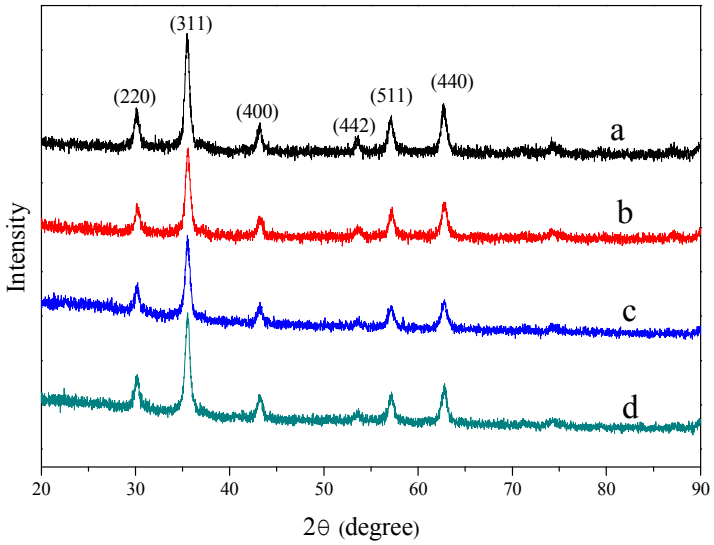

587

588 **Fig. 1** XRD patterns of (a) Fe_3O_4, (b) Fe_3O_4@SiO_2, (c) Fe_3O_4@SiO_2-mPD/SP(95:5)

589 and (d) Fe_3O_4@SiO_2-mPD/SP(50:50).

590

591

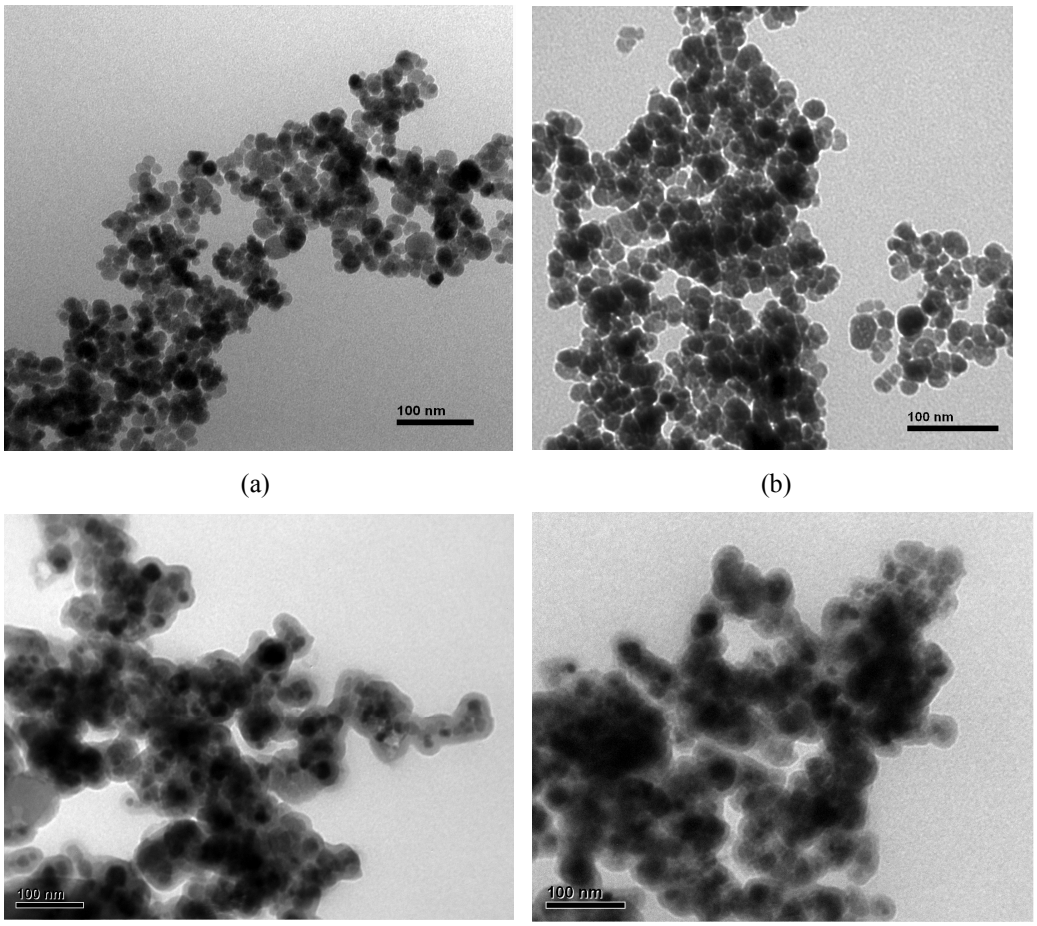

(a) (b)

(c) (d)

592 **Fig. 2** TEM images of (a) Fe_3O_4, (b) Fe_3O_4@SiO_2, (c) Fe_3O_4@SiO_2-mPD/SP(95:5)

593 and (d) Fe_3O_4@SiO_2-mPD/SP(50:50).

594

595

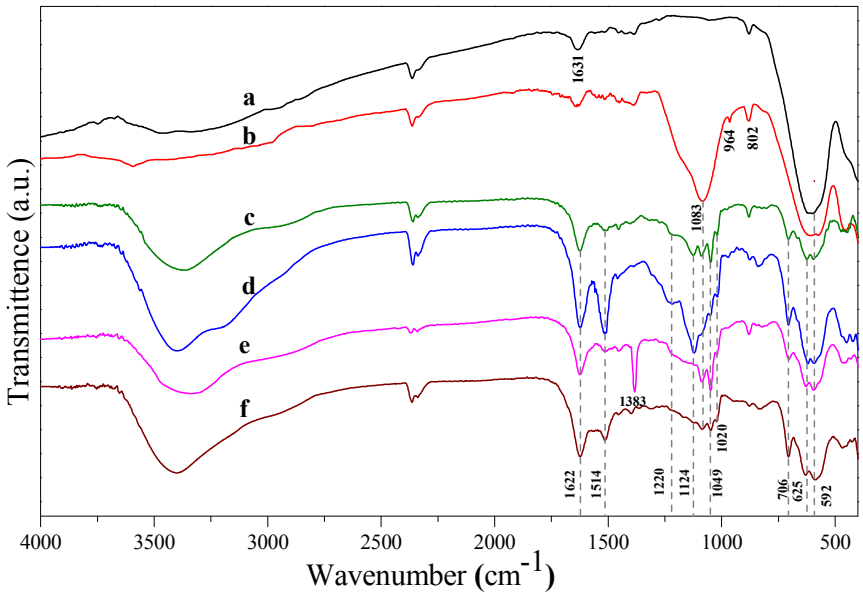

596

597 **Fig. 3** FTIR spectra of (a) Fe_3O_4, (b) Fe_3O_4@SiO_2, (c) Fe_3O_4@SiO_2-mPD/SP(95:5),

598 (d) Fe_3O_4@SiO_2-mPD/SP(50:50), (e) Fe_3O_4@SiO_2-mPD/SP(95:5) after adsorption of

599 Pb(II), and (f) Fe_3O_4@SiO_2-mPD/SP(50:50) after adsorption of Cr(VI).

600

601

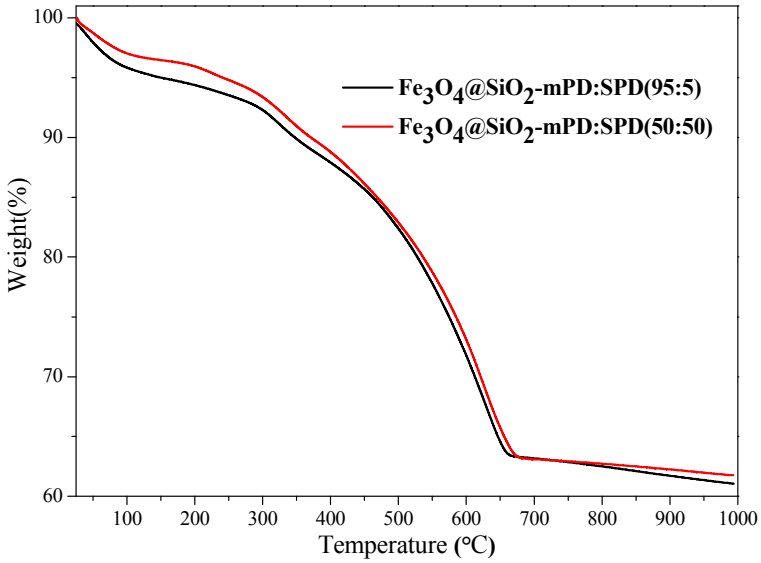

602

603 **Fig. 4** TGA curves of Fe_3O_4@SiO_2-mPD/SP(95:5) and Fe_3O_4@SiO_2-mPD/SP(50:50).

604

605

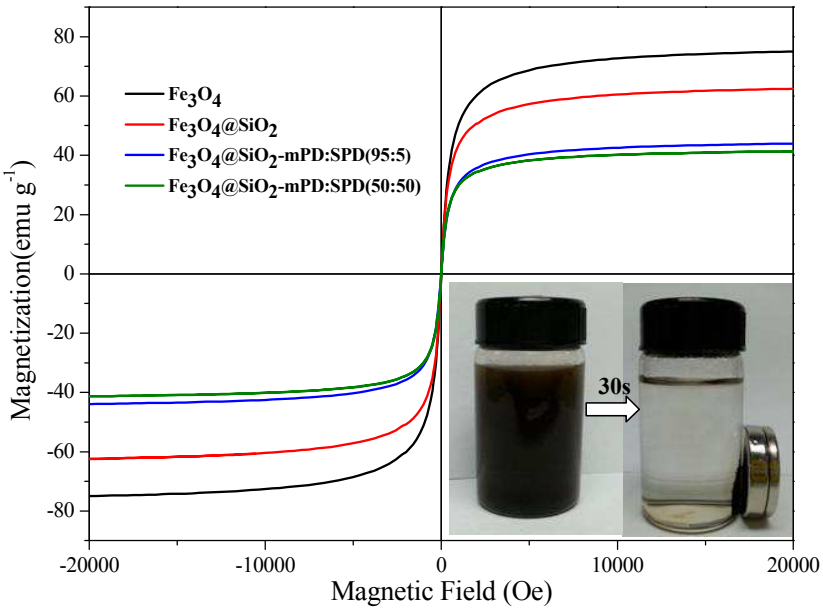

606

607 **Fig. 5** Magnetization curves of Fe_3O_4, Fe_3O_4@SiO_2, Fe_3O_4@SiO_2-mPD/SP(95:5) and

608 Fe_3O_4@SiO_2-mPD/SP(50:50).

609

610

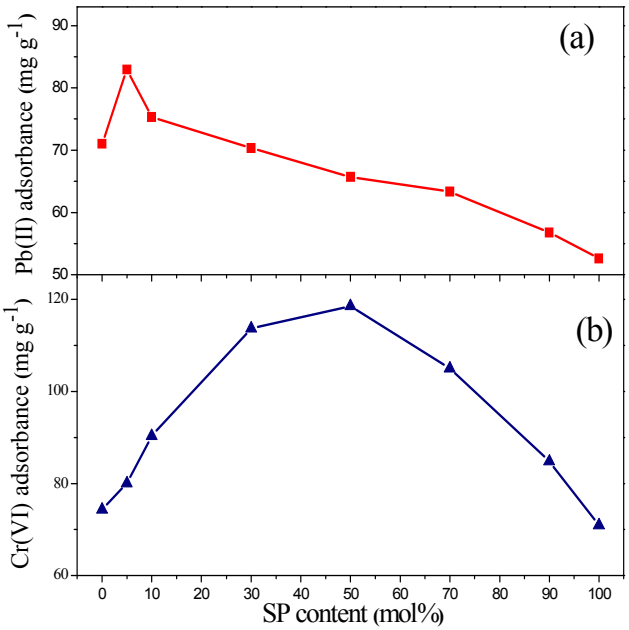

611

612 **Fig. 6** (a) Pb(II) adsorptivity at an initial Pb(II) concentration of 100 mg L^{-1}, (b) Cr(VI)

613 adsorptivity at an initial Cr(VI) concentration of 150 mg L^{-1} with the same 1 g L^{-1}

614 Fe_3O_4@SiO_2-mPD/SP nanocomposites at 30°C for 24h.

615

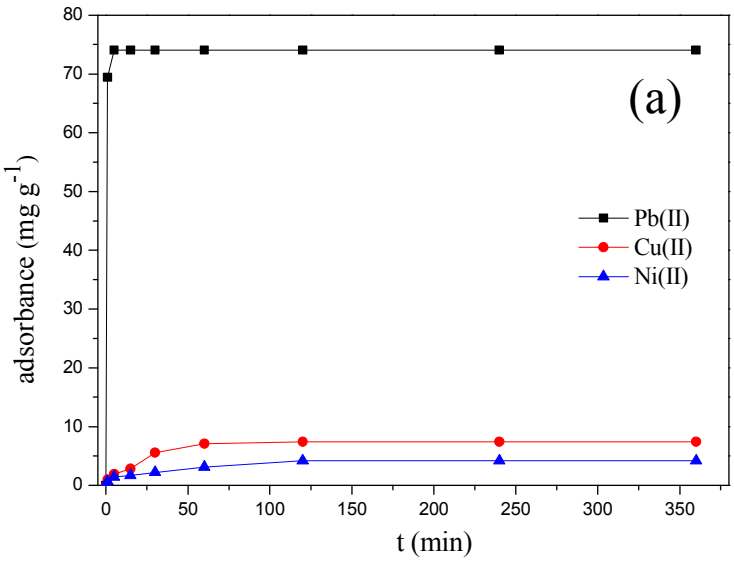

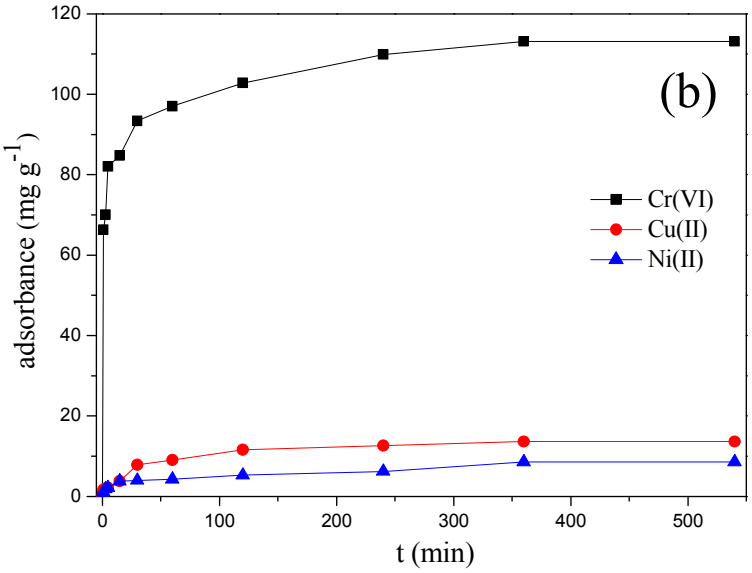

616 **Fig. 7** Selective adsorption of Pb(II) and Cr(VI) onto Fe_3O_4@SiO_2-mPD/SP
617 nanocomposites: (a) adsorption of Pb(II), Cu(II) and Ni(II) by
618 Fe_3O_4@SiO_2-mPD/SP(95:5) at an initial single ion concentration of 100 mg L^{-1}, (b)
619 adsorption of Cr(VI), Cu(II) and Ni(II) onto Fe_3O_4@SiO_2-mPD/SP(50:50) at an initial
620 single ion concentration of 150 mg L^{-1}, with the same 1 g L^{-1} Fe_3O_4@SiO_2-mPD/SP
621 nanocomposites at 30°C.

622

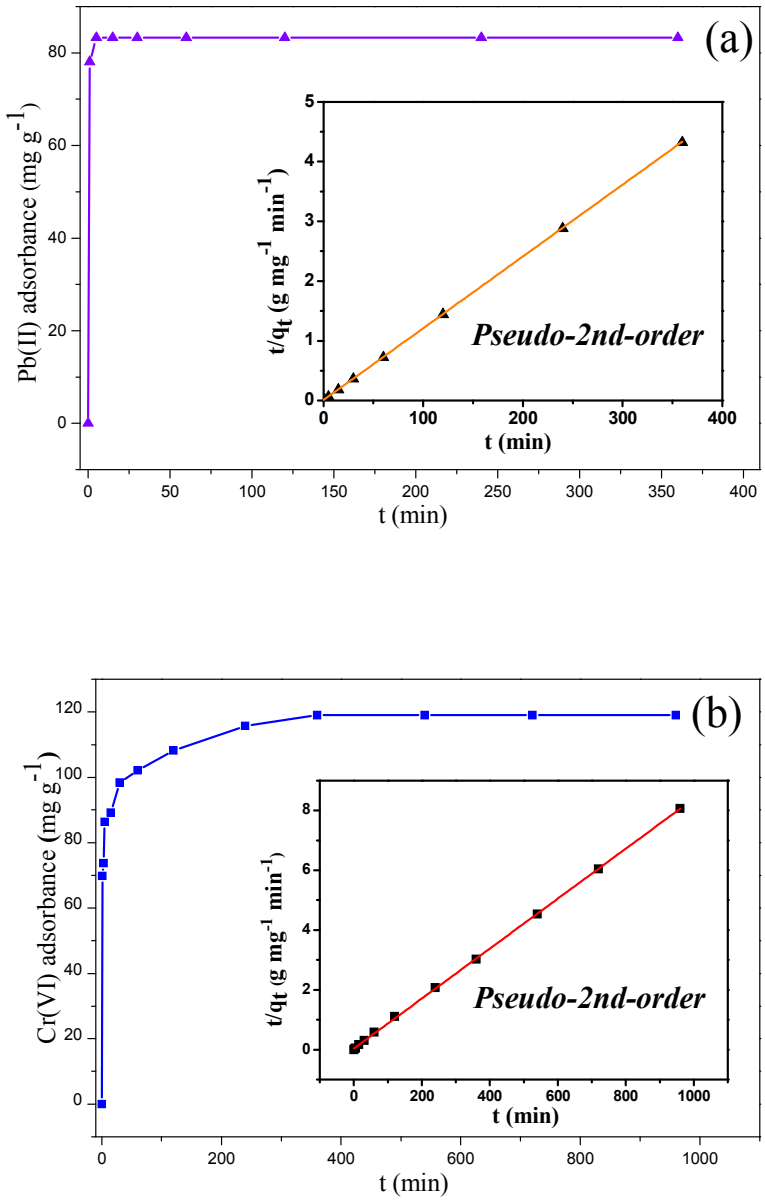

623 **Fig. 8** Effect of contact time on Pb(II) adsorption onto Fe_3O_4@SiO_2-mPD/SP(95:5)
624 (a), and Cr(VI) adsorption on Fe_3O_4@SiO_2-mPD/SP(50:50) (b). Pb(II) initial
625 concentration = 100 mg L^{-1}, Cr(VI) initial concentration = 150 mg L^{-1},
626 Fe_3O_4@SiO_2-mPD/SP nanocomposites = 1 g L^{-1}, 30°C.

627

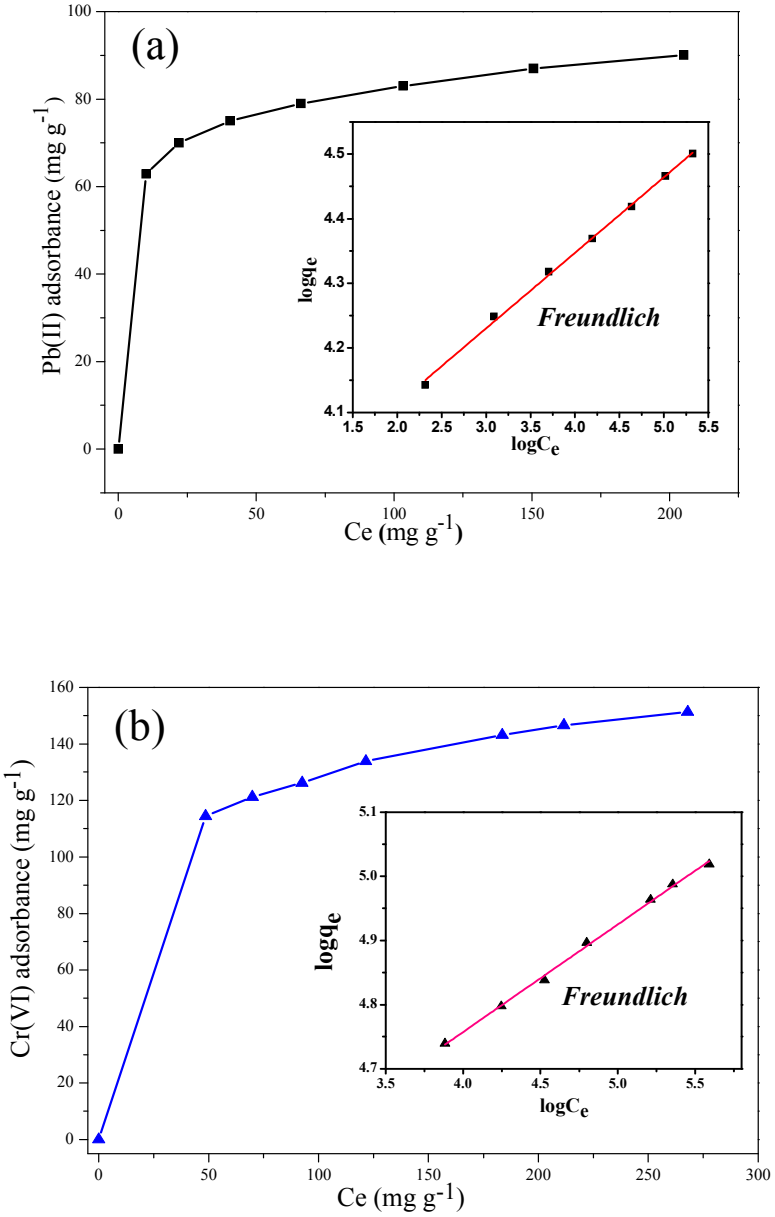

628 **Fig. 9** Equilibrium isotherm for the Pb(II) adsorption onto Fe_3O_4@SiO_2-mPD/SP(95:5)

629 (a), and Cr(VI) adsorption on Fe_3O_4@SiO_2-mPD/SP(50:50) (b) with the same 1 g L^{-1}

630 Fe_3O_4@SiO_2-mPD/SP nanocomposites at 30°C. The inset illustrates the linear

631 dependence of logqe on logce.

632

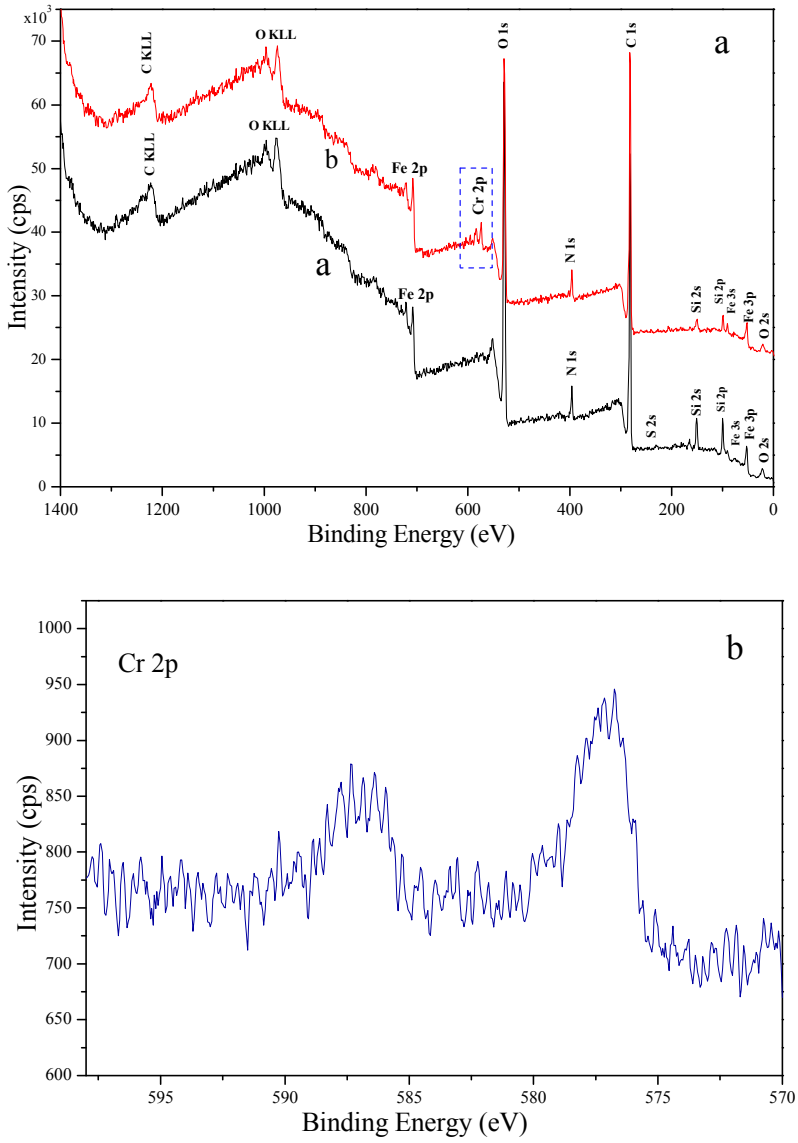

633 **Fig. 10** XPS wide survey for Fe_3O_4@SiO_2-mPD/SP(50:50) before and after Cr(VI)

634 adsorption (a). High-resolution XPS survey of Cr2p (b).

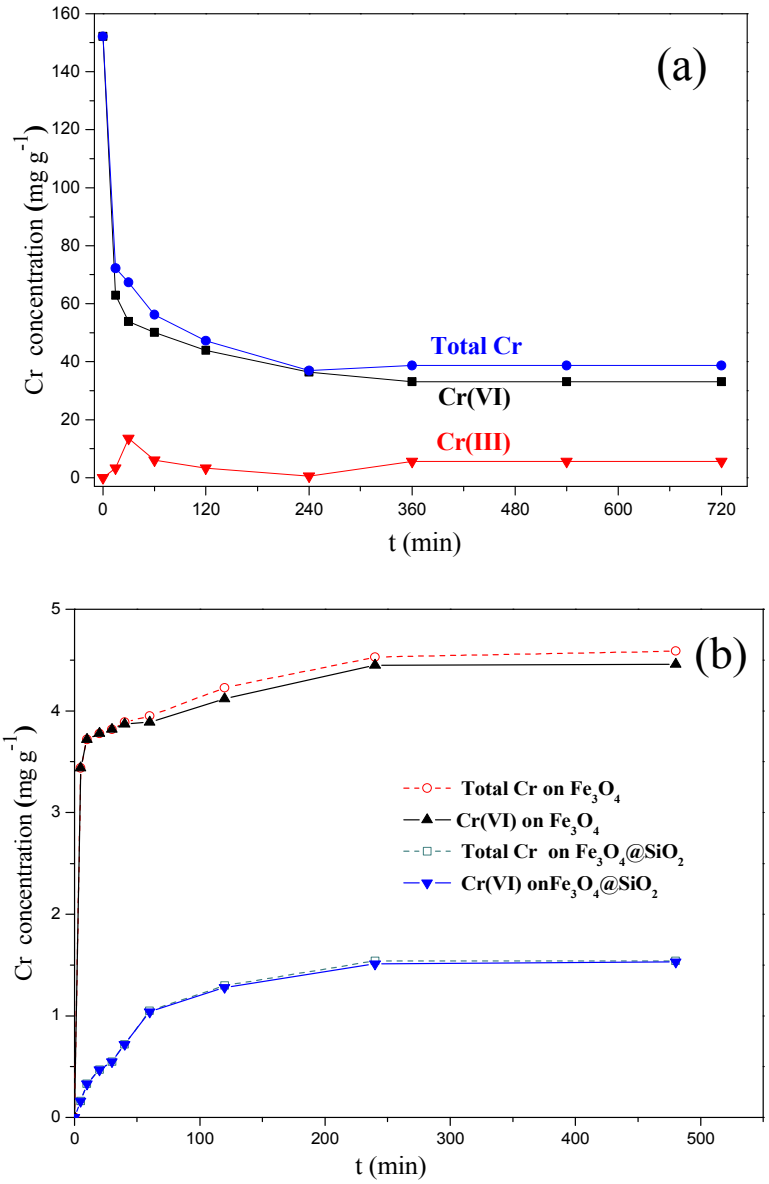

635 **Fig. 11** (a) The variation of residual concentration of total Cr and Cr(VI) with
636 adsorption time onto Fe_3O_4@SiO_2-mPD/SP(50:50). (b) The variation of residual
637 concentration of total Cr and Cr(VI) with adsorption time onto Fe_3O_4 and
638 Fe_3O_4@SiO_2.
639

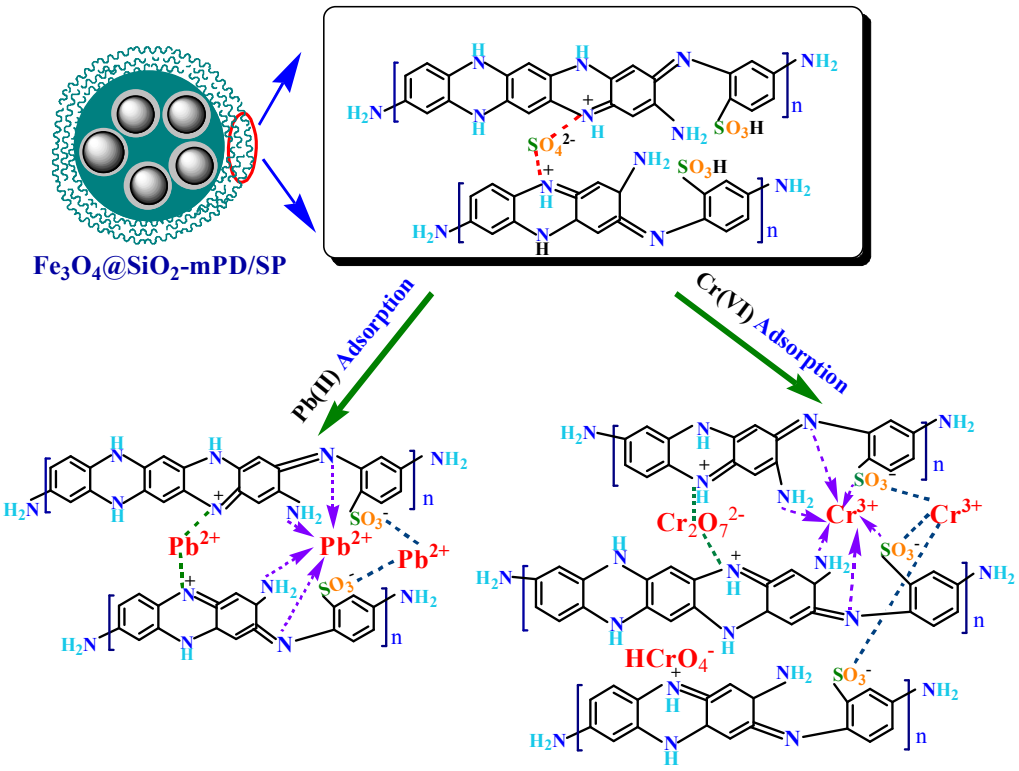

640
641

642 **Fig. 12** The possible Pb(II) and Cr(VI) adsorption mechanism on

643 Fe_3O_4@SiO_2-mPD/SP nanocomposites.